Single Shot Single Antenna Path Discovery in THz Networks

Yasaman Ghasempour
Rice University
ghasempour@rice.edu

Chia-Yi Yeh
Rice University
cy20@rice.edu

Rabi Shrestha
Brown University
rabi_shrestha@brown.edu

Daniel Mittleman
Brown University
daniel_mittleman@brown.edu

Edward Knightly
Rice University
knightly@rice.edu

ABSTRACT

THz communication has the potential to realize an order of magnitude increase in data rates due to the availability of wide THz-scale spectral bands. Unfortunately, establishing and managing highly directional beams in THz networks is challenging as links lack the "pseudo-omni" reception capability of lower bands and the product of AP-client beam resolution is high due to narrow beams of only a few degrees. In this paper, we present *One-shot Path discovEry with a THz RAinbow (OPERA)*, a novel system that identifies dominant paths between the AP and all clients in order to efficiently steer directional beams. The key idea is to embed path direction into the inherent characteristics of signals traveling along each path. To do so, we exploit a *single leaky wave antenna* and create a *THz Rainbow*. A THz Rainbow transmission consists of distinct signals with unique spectral characteristics across the angular domain. Leveraging the spatial-spectral signatures in the THz Rainbow, all receivers can correlate the measured signal with the known transmission signatures to discover the sender's path directions in *one-shot*. Our experiments demonstrate that OPERA achieves average direction estimates within 2° of ground truth for LOS and reflected paths.

CCS CONCEPTS

• **Networks → Network protocol design**; *Wireless local area networks*; Mobile networks.

KEYWORDS

Terahertz, Path Discovery, Beam Steering, Leaky Wave Antenna

ACM Reference Format:
Yasaman Ghasempour, Chia-Yi Yeh, Rabi Shrestha, Daniel Mittleman, and Edward Knightly. 2020. Single Shot Single Antenna Path Discovery in THz Networks. In *The 26th Annual International Conference on Mobile Computing and Networking (MobiCom '20), September 21–25, 2020, London, United Kingdom.* ACM, New York, NY, USA, 13 pages. https://doi.org/10.1145/3372224.3380895

MobiCom '20, September 21–25, 2020, London, United Kingdom

ACM ISBN 978-1-4503-7085-1/20/09…$15.00
https://doi.org/10.1145/3372224.3380895

1 INTRODUCTION

Driven by increased spectrum availability at 60 GHz, multi-Gb/sec wireless transmission is now feasible and is already standardized in IEEE 802.11ad/ay [7, 23]. Scaling spectrum access towards the terahertz (THz) regime, from 0.1 to 1 THz, can realize the next order of magnitude in data rate due to the availability of even wider spectral bands. However, efficient coordination of *spatial* resources is a fundamental challenge in THz-scale networks with highly directional beams. In particular, given that THz links lack the "pseudo-omni" reception capability available at millimeter wave, techniques from [7, 23] cannot be applied. Moreover, due to their inherently more directional nature (narrow beams of only a few degrees [6] as opposed to tens of degrees in mmWave beams [28, 31]), the number of possible sender-receiver beam pairs is significantly increased, rendering the overhead of exhaustive testing infeasible.

In this paper, we present OPERA, One-shot Path discovEry with a THz RAinbow, a novel system that identifies high-rate physical paths between the Access Point (AP) and all clients via a single-shot THz pulse transmission. Due to high path loss in THz bands, only a few dominant paths exist between a pair of nodes, e.g., one line-of-sight (LOS) path and possibly a small number of reflected paths.

Our key idea is to transmit distinct signals with unique signatures across different angles such that each physical path has its own signature. To create a unique signature in each direction *simultaneously*, we introduce a novel THz node architecture in which the AP and clients are equipped with a Leaky Wave Antenna (LWA).[1] A LWA allows traveling wave to leak from a waveguide into free-space with the unique property that the emission angle from the waveguide is coupled to the frequency of the input signal via a simple closed form and monotonic relationship [13]. We exploit this property in new ways and develop the *first* LWA-based path discovery system: First, we create a "THz Rainbow" by exciting the LWA with a time-domain THz pulse (equivalently, a broadband signal in frequency-domain) such that the signal emitted at each angle has a unique signature, thus filling the entire angular space with signal. Namely, each direction has a unique spectral peak or "color" due to the LWA's frequency-angle coupling. Second, in addition to its spectral peak, known from [13], we discover that each direction also has a unique spectral *signature*. Consequently, we develop a model for predicting the angle-dependent spectral signature, based on the physics of EM

[1] We interchangeably use leaky waveguide and leaky wave antenna in this paper.

waves propagating through and emitting from LWAs. The model is a deterministic function of the LWA geometric properties and thus can be known *a priori* by the AP and clients. With this design, the receiver can correlate its received portion of the THz Rainbow with the known transmission signatures, thereby identifying the transmission direction of each of the sender's paths.

Our design is a non-coherent path discovery scheme in that it only requires power measurement at the receiver, and not phase information. This relaxation simplifies the THz node architecture, eliminates the need to keep tight synchronization between the transmitter and receiver, and is robust to small-scale channel variation (as opposed to phase with substantial sensitivity to sub-millimeter scale movement in the THz regime). Moreover, path discovery in OPERA is scalable, such that *all* clients can simultaneously and independently identify their LOS and NLOS paths via analyzing their received power spectrum from a single-shot transmission of the THz pulse shaped by a LWA.

Leveraging the design of OPERA, we present the *first single shot single antenna path discovery system in THz networks*. We implement the key components of OPERA on a THz testbed and perform extensive over-the-air experiments in various settings. Our testbed consists of a THz pulse generator, broadband receivers, and custom LWAs. Our key findings are as follows:

(i) We experimentally demonstrate a THz Rainbow for the first time and measure its complex spatial-spectral profile. We find that any frequency component within the bandwidth of source emerges from the LWA in a range of emission angles, including but not limited to the angle known from literature [13]. In addition, we observe that the angular span of such emissions is itself frequency-dependent causing a unique spatial-spectral signature at each direction.

(ii) Even though the spectral peak has a one-to-one relationship with emission angle, our experiments reveal that discovering paths solely via this relationship incurs critical limitations: (1) estimation accuracy is not robust across the entire angular range and (2) reflected paths non-uniformly impact power over different frequencies which can lead to a spectral peak shift and subsequent estimation inaccuracy.

(iii) Instead, OPERA takes advantage of the unique spatial-spectral signatures of the THz Rainbow and achieves average estimation error of $< 1.1^\circ$ for the first path and $< 1.9^\circ$ for the second path.

(iv) Moreover, we exploit the path directions provided by OPERA to adapt directional THz beams under client mobility. We find that the non-zero error in path estimates causes slightly misaligned beam steering and subsequent SNR penalty of 0.29 dB on average. Yet, as the time interval between two path discovery measurements increases, the corresponding SNR loss becomes larger. Interestingly, our analysis shows that the time overhead of a THz Rainbow is orders of magnitude smaller than regular client mobility time-scales. Hence, the overhead of OPERA, even if executed before every data transmission, is relatively small.

The rest of this paper is organized as follows: Sec. 2 illustrates our system architecture. Sec. 3 presents the design of OPERA. Sec. 4 introduces our experimental platform and Sec. 5 describes the evaluation results. Sec. 6 reviews the related work and Sec. 7 concludes this paper.

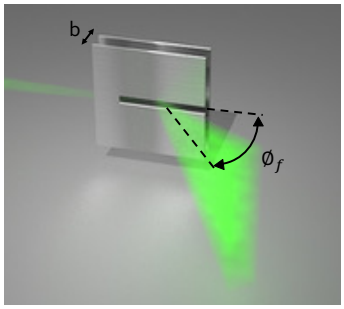

Figure 1: A Leaky Wave Antenna in which the input signal emerges from the slot such that the maximum emission angle ϕ_f is related to input frequency via Eq. (1). The larger the input frequency, the lower the emission angle relative to the plate's axis.

2 SYSTEM ARCHITECTURE

In this section, we provide background on LWAs and introduce our THz control plane architecture.

2.1 Primer on Leaky Wave Antennas

A LWA consists of a pair of parallel metal plates with open sides and a slot in one of the metal plates. Fig. 1 depicts a LWA device with separation b between its two metal plates. By opening a single slot in one of the two plates, we permit some of the radiation to "leak" out into free space.

Angle-Frequency Relation. The energy emitted at a particular angle is a function of input frequency with the overall emission pattern known to be very complex. With some simplifications, Maxwell's equations with boundary conditions between the waveguide mode and free space mode yield a direct relation between the maximum emission angle and the frequency of the input signal [9]. For the lowest transverse-electric mode, we can derive [15]:

$$\phi_f = sin^{-1}\left(\frac{c}{2bf}\right), \tag{1}$$

where f is the frequency of the input signal, c is the free-space light speed, and b represents the distance between the two metal plates. Other geometrical parameters, such as the width and length of the leaky-wave aperture, can impact the efficiency of energy transfer between the guided mode and free-space, but not the maximum-energy emission angle. The subscript f in ϕ_f emphasizes that, given a fixed LWA structure, this angle is solely a function of input frequency. Moreover, Eq. (1), which we also refer to as a first principle model, suggests that the larger the input frequency, the lower the emission angle from the slot.

Conversely, when operated as a receiver, free-space waves with the frequency f would couple best into the waveguide if they are arriving at the slot with the correct angle ϕ_f. Thus, one can expect a simple and monotonic relationship between frequency and maximum-energy angle, for both the case of a guided wave radiating into free space and the case of a free-space wave impinging on the device and coupling to a guided wave (i.e., for both transmission and reception of signals).

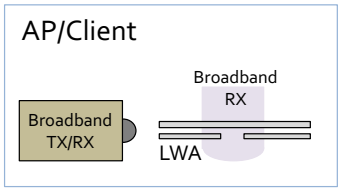

Figure 2: The control plane architecture consisting of a LWA, a broadband transceiver, and a broadband RX.

2.2 Node Architecture

We exploit LWAs in the control plane to discover dominant paths in highly directional THz channels. We equip both the AP and client with LWAs. Fig. 2 depicts the core of our proposed node architecture which consists of a LWA antenna, a broadband receiver (co-located with the LWA), and a broadband transceiver that can generate THz pulses or detect broadband (up to 1 THz) signals. In transmission mode, the injected signal to the LWA leaks out with an emission that falls within a sector of 90°, depending on the frequency of the signal. In reception mode, the waves are coupled into the waveguide and then guided toward the broadband receiver located at end of the metal plates.

Note that Fig. 2 shows the control plane architecture only. For data transmission, nodes can use another beam steering architecture (such as phased-array architecture in [29] or pixelated metasurface structures in [14]). We consider that such data plane components are either co-located with the LWA or their geometrical properties are known so that we can directly map the discovered paths in the control plane to the data plane.

Deployment Costs. LWA structures are passive, light (<3 oz), and cheap (<$10) and can easily meet the power, size, weight, and cost considerations of future handheld devices. Further, THz broadband transceivers have been designed and implemented using CMOS-technology in prior work [4]. With CMOS-technology, the cost of a broadband transceiver in the THz regime would not be significantly higher than today's commercialized transceivers in lower bands. Hence, we anticipate that the large-scale deployment of OPERA would not raise any significant cost concerns.

Towards 360° Coverage. Our system uses a single LWA to transmit within a sector of 90 degrees. The angular range can be increased to 360° by extending the node architecture. In particular, employing a multi-face LWA structure increases the angular coverage. Yet, simultaneous transmissions from multiple LWAs raises an ambiguity concern for the receiving node, who may not be able to tell from which LWA a detected signal originated. One way to tackle this issue is to exploit an additional degree of freedom in LWAs (e.g., the shape of the leaky-wave slot, which need not have a constant width along its length) to generate transmission patterns with slightly different spectral-spatial signatures for each segment. Building and testing a multi-face LWA structure would be an interesting engineering problem that we leave for future work. Here, for ease of exposition, we limit scope to one 90° sector.

3 OPERA DESIGN

In this section, we describe the design of OPERA that aims to discover dominant physical paths in THz channels in a single shot and using a single antenna.

3.1 Design Overview

The higher path loss in THz frequency range necessities the use of directional beams at both sender and receiver. The best directions to transmit are typically unknown in advance and thus different directions need to be tested for their achievable signal strength. In most systems, the receiver needs to be explicitly informed of each direction the transmitter is testing so that it can notify the sender which direction was best. For instance, in directional 60 GHz WLANs, IEEE 802.11ad specifies a beam sweeping mechanism in which beacons are transmitted with an explicit and unique header in each direction [23]. Such a scheme involves several consecutive beacons to cover all possible directions and hence the time overhead increases with the total number of directions.

We propose OPERA, a single-shot single-antenna path discovery platform that identifies high-rate physical paths between the AP and clients. THz channel sparsity suggests that only a few dominant high-rate paths (LOS and possibly first-order reflected paths) exist between any two nodes [20]. Our key idea for path discovery is to embed path information into the inherent characteristics of the signal traveling along that path. In particular, we enable the receiver to correlate the sender's path direction with the spectral signature of the signal transmitted in that direction. For instance, one naive LWA implementation would be to deploy a beam sweeping mechanism analogous to that of IEEE 802.11ad, but vary the carrier frequency of beacons transmitted in different directions. Even though such an approach would assign unique spectral signatures (i.e., carrier frequency) to different directions, it would not be a single-shot scheme as several consecutive transmissions would be involved.

Instead, we show how to use a single leaky waveguide antenna for efficient single-shot path discovery. In particular, we deploy a LWA device and introduce a *THz Rainbow* to simultaneously transmit waves whose spectral characteristics are a function of emission angle. While it may seem that obtaining the peak frequency as the direction dependent signature (i.e., angle-frequency coupling in Eq. (1)) would be sufficient for path discovery, our experimental analysis shows that this is not the case. Hence, we introduce a phenomenological model to characterize the angular-dependent spectral signature of waves composing THz Rainbow. Leveraging this model, we devise an optimization framework to extract the unique features of multiple distinct paths from the received power spectrum.

Finally, OPERA is an incoherent scheme, i.e., it solely relies on the power or signal strength measurement (and not phase information) to estimate the path angles. To exploit phase, the transmitter must first send a pre-defined preamble in order for the receiver to lock on to the phase; in contrast, OPERA eliminates the need to keep tight synchronization between TX and RX. Moreover, it is robust to small-scale channel variation as opposed to phase with substantial sensitivity to sub-millimeter scale movement in THz regime. Next, we illustrate the key components of OPERA.

3.2 THz Rainbow

Leaky wave antennas have a long history, having been used in the RF region since at least the 1940's [2] and more recently, in the THz regime [15]. However, this work is the first to employ LWAs as a control plane for the THz WLANs. We propose, for

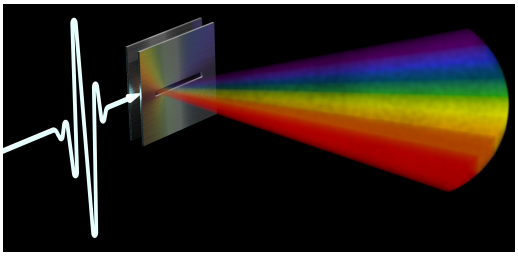

Figure 3: Creation of a THz Rainbow by exciting a LWA device with a THz pulse.

the first time, to excite a LWA with a THz pulse. THz pulse generation and its conventional applications in spectroscopy has been studied in prior work [3]. Here we excite the LWA with a THz pulse source (or equivalently, an ultra-broadband input signal in frequency-domain).[2] Due to the angle-frequency coupling in a LWA, different frequency components are decomposed and radiated into the free-space at different angles forming what we call a "THz Rainbow."

In this scheme, the entire space is filled with THz signals such that different frequencies (within the bandwidth of the source) simultaneously directed to different angles across the entire angular range. Fig. 3 depicts the THz Rainbow with angular dependency in the spectral signature of radiating signals. In particular, in lower angles (relative to the axis of the LWA), the radiating waves contain higher frequency components and are fast decaying in the time-domain. In contrast, waves emitting at larger angles are wider in the time-domain and have relatively smaller frequency components. A broadband receiver in the far field of the LWA captures only a portion of the THz Rainbow. Thus, OPERA takes hints from the received signal to estimate the angles of departure and arrival corresponding to the LOS and all reflected paths between a TX and RX.

As a result of diffraction from the finite LWA aperture, emission of waves from LWA to free-space spans in 3D (see Fig. 1 for the emission of a single-frequency signal). Although not shown in Fig. 3, the THz Rainbow has a 3D transmission pattern. Hence, in principle, we can extend the spatial-spectral signatures and mathematical formulation to extract both azimuth and elevation angles from the received signal. We leave exploration of single-shot 3D path discovery with THz Rainbow for future endeavors and focus on 2D path discovery in this paper.

3.3 The Angular-Dependent Spectral Signature of the THz Rainbow

In order to relate the received signal to the properties of the underlying physical paths (e.g., AoA and AoD), we need to characterize the mediums in which waves propagate to reach the RX. Fig. 4 depicts different components of an end-to-end channel between the source and RX: An input signal is guided inside the LWA until it radiates out of the slot. We assume propagation inside the LWA is ideal. While the waveguide introduces some dispersion (since this is a transverse electric waveguide mode) and loss (since the plates are made of real metals with non-infinite conductivity),

[2]In our platform, the 3 dB bandwidth of the broadband source is 1 THz.

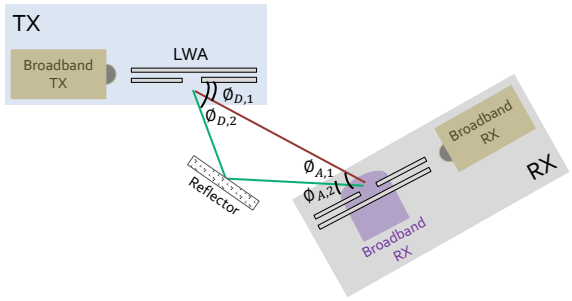

Figure 4: The end-to-end channel between a broadband source and a broadband RX.

both of these effects are quite small [18]. However, radiation from the LWA to the air imposes spatially-biased attenuation. The signal subsequently traverses the available paths of the wireless medium. Finally, impinging wave are coupled into the LWA and guided toward the RX.

For radiation out of the waveguide into free-space, we know the relation between spectral peak and emission angle from Eq. (1). However, our measurements show that any specific frequency component is not a spatial delta function. Instead, the power spectrum of signals leaking from the waveguide can appear at a range of angles, albeit encountering different coupling losses. More importantly, our measurements indicate that the angular width of the signal at any particular frequency is frequency dependent.

To understand this broader angular width, we analyze the underlying physical properties of leaky waves. We treat the leaky waveguide slot as a finite-length aperture, which produces a diffraction pattern in the far field. In this case, the angular distribution of the diffracted field (in the plane of the slot) can be derived for a given frequency f by treating the slot as a diffracting aperture of length L, such that the far-field pattern is the Fourier transform of the aperture function [9]:

$$G(\phi, f) = sinc[(\beta - j\alpha - k_0 cos\phi)\frac{L}{2}] \tag{2}$$

where k_0 is the free-space wave vector ($k_0 = \frac{2\pi f}{c}$), β is the wave vector of the TE_1 guided wave ($\beta = k_0\sqrt{1-(\frac{c}{2bf})^2}$), and α is a parameter that describes the loss of energy in the guided mode due to leakage out of the slot. Note that for $\alpha \ll \beta$, the peak value of $G(\phi, f)$ happens at $cos\phi = \frac{\beta}{k_0}$ which is the same as Eq. (1) except for a change in the angle definition. Note that Eq. (2) suggests that the diffraction pattern is not a function of transmitter-receiver distance.

While the rigorous diffraction formulation in Eq. (2) accurately describes the far-field radiation pattern, it is cumbersome to use as a fitting function, in particular because the side lobes associated with a sinc function fall below the dynamic range of our measurement system, and are therefore not observed in our data. Further, for the purpose of path discovery, the high-amplitude portion of the signature plays the key role. Hence, as an alternative, we introduce a second-order phenomenological model which is meant to characterize the high-amplitude spectral characteristics incorporating the observations from our measurements. For a given frequency f, we model LWA emission as a spatial filter or a directional radiation pattern with highest directivity along

the previously predicted peak angle, and fall off on both sides. We model this behavior as a filter that is a symmetric parabolic function of angle ϕ:

$$\tilde{G}(\phi, f) = max(1 - \gamma(f)(\phi - \phi_f)^2, 0), \quad (3)$$

where ϕ_f is the maximum-energy angle corresponding to frequency f as defined in Eq. (1). The filter function $\tilde{G}(\phi, f)$ models the fraction of amplitude at frequency f that is emitted at angle ϕ w.r.t. the LWA's metal plate. At the center of the filter, i.e., at the optimum angle ϕ_f, the power is maximum and $\tilde{G}(\phi_f, f) = 1$. As we deviate from the optimum angle, power is attenuated with a frequency-dependent rate denoted as $\gamma(f)$. Specifically, our data indicates that the fall-off rate $\gamma(f)$ can be represented as a linear function of frequency such that the angular width becomes narrower as frequency increases. With a linear $\gamma(f)$ function, namely, $\gamma(f) = \gamma_0 + \gamma_1 f$, we have only two parameters to fit a family of quadratics. There is no closed-form expression available for $\gamma(f)$; yet, for a fixed node architecture (i.e., a given LWA geometry), it is a deterministic function of frequency which can be measured and known *a priori*.[3]

For angles ϕ far from ϕ_f, $1 - \gamma(f)(\phi - \phi_f)^2$ becomes negative. For these values of ϕ, we assume that there is zero power detected (i.e., the signal simply misses the detector), and so we set $G = 0$. In Sec. 5, we validate this LWA-to-air emission model. Now that we have modeled the transmission pattern of a THz Rainbow, we can proceed to path discovery by exploiting the known and fixed THz Rainbow pattern as angular-spectral signatures.

3.4 One Shot Path Discovery

We envision periodic THz Rainbow excitation so that receivers are able to update their angular profile by assessing the received power spectrum. Next, we illustrate OPERA's AoD and AoA estimation techniques.

3.4.1 AoD Estimation. The THz Rainbow is composed of signals in all directions within a sector of 90°. However, only signals along the dominant paths of the over-the-air wireless channel can reach the receiver. Each path contributes to the power spectrum depending on its angular-dependent spectral signature. Hence, we can model the total power spectrum based on the aggregated effect of signals from all paths reshaped by the LWA spatial filter gain:

$$S(f) = |\sum_{p=1}^{P} \tilde{G}(\phi_{D,p}, f)\alpha_p(f)|^2 \quad (4)$$

where P is the number of multipath components, $\phi_{D,p}$ denotes the AoD corresponding to path p, and $\alpha_p(f)$ represents the complex wireless channel gain over path p.

While Eq. (4) models the expected power spectrum based on path directions, we can also measure the actual received power spectrum at our broadband detector. In practice, power measurements are available over a discrete set of frequencies depending on the clock sampling rate. We denote $\mathbf{S^{ms}}$ as the vector of power measurements across the available set of frequencies. Similarly, $\mathbf{S}$ captures the expected power spectrum based on Eq. (4) computed for the same set of frequencies. Note that $\mathbf{S}$, by definition, is a sparse tall vector as $\tilde{G}(\phi_{D,p}, f_i)$ is zero for frequencies far from the peak frequency corresponding to $\phi_{D,p}$. Hence, we estimate the AoD that best describes the power measurements across the entire spectrum:

$$\phi^*_{D,1} = \arg\min_{\phi} ||\mathbf{S} - \mathbf{S^{ms}}||^2 \quad (5)$$

where $\phi^*_{D,1}$ is the estimate angle of the strongest path. OPERA assumes that other paths, if present, are significantly weaker such that the received signal signature is dominated by the spectral signature of the strongest path. Once the strongest path is identified, we remove its spectral signature from the measured power spectrum $\mathbf{S^{ms}}$ and repeat the optimization in Eq. (5) to discover the second path. OPERA stops this iterative process when the power to noise ratio of the residual signal drops below a configurable threshold. We emphasize that no phase information is used in this methodology, hence the detector can be non-coherent.

3.4.2 Opportunistic AoA Estimation. In principle, assuming that the THz wireless channel is reciprocal, AoA can be estimated similarly by generating a THz Rainbow at the client and assessing the received spectrum at the AP. Potentially, we can take advantage of the receiver's node architecture to opportunistically estimate AoA, at least for a range of angles, without initiating a separate THz Rainbow. Namely, comparing the spectral characteristic of impinging waves at the LWA before and after coupling into the waveguide provides insights on the AoA. Intuitively, if the client's LWA is parallel to the AP's LWA (i.e., AoD=AoA), then the air-to-waveguide coupling loss is negligible and we expect a similar spectral characteristics for coupled and impinging waves. However, when the AoA is different from AoD, then the coupled waves would experience a frequency-dependent power loss that can be exploited to extract the AoA. Of course if the AoA is far from AoD, one would expect that the client would receive no signal. However, our preliminary analysis shows that the spectrally broader emission at a specific angle enables a fairly large |AoA-AoD| without complete loss of signal. In any case, the client can always generate a THz Rainbow and repeat the mechanism described above to explicitly estimate the AoA of the dominant paths. In our experiments, we focus on evaluation of AoD/AoA with the explicit THz Rainbow generation and we leave the exploration of opportunistic AoA estimation and its limitations for future work.

3.4.3 Overhead Analysis. The AP periodically generates the THz Rainbow while all clients measure the received signal with their broadband detectors to update their path profiles. We denote T_{rb} as the cycle duration of THz Rainbow transmissions. A smaller T_{rb} indicates that path information updates are available more frequently with the cost of higher time overhead. However, we argue that even if we update path information before every data packet transmission, the interference and overhead costs are insignificant:

First, THz Rainbow transmission incurs negligible overhead, in the range of few tens of nano second depending on the THz pulse generation method [4] whereas mobility is in millisecond scale. This means that to manage regular client mobility (e.g., walking or running speed), path information needs to be updated, at most, in sub-millisecond scale while OPERA is orders of magnitude faster,

[3]For our particular LWA structure, we find $\gamma(f) = 0.032f + 0.01$, when frequency is in THz unit and angle is in degrees.

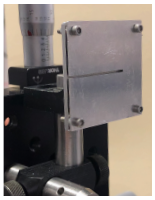

Figure 5: Our custom $4 \times 4\ cm^2$ LWA.

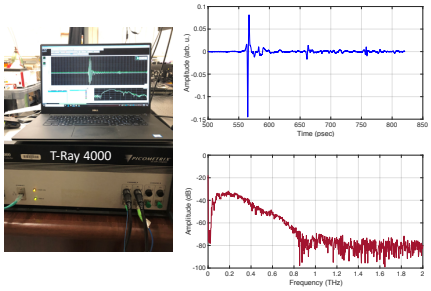

Figure 6: The ultra-broadband transceiver system and its generated THz pulse in time and frequency domains.

causing the ratio of control plane overhead to data transmission to be negligible. Moreover, OPERA has a scalable design such that all clients can simultaneously and independently update their AoD information via a single sender-side THz Rainbow transmission.

Second, it may seem that OPERA is a resource-intensive solution since it fills the entire space with THz signals composed of a broad range of frequencies that may cause interference with any on-going transmissions in neighboring cells. However, the THz Rainbow transmission only takes several nano seconds and not every frequency component exists in every direction. In fact, interference can take place only if a node in a neighboring cell is located at a specific angle and operates in a frequency band that matches the LWA angle-frequency relation. In other words, the footprints of the THz Rainbow are narrow in space and short in time. Further, as this transmission is broadband, the power of different sub-bands is limited and thus the signal is unlikely to be received at longer distances of neighboring cells. However, in an extreme case, the APs could coordinate to minimize the inter-cell interference.

4 EXPERIMENTAL PLATFORM

We conduct extensive over-the-air experiments to characterize the THz Rainbow and evaluate the performance of OPERA. We exploit a custom LWA device, shown in Fig. 5, which we build using $4 \times 4\ cm^2$ metal plates and 1.075 mm spacers in between (i.e., plate separation $b = 1.075$ mm). Other geometrical parameters include the plate thickness (1 mm), the slot length (3 cm), and the slot width (1 mm).

For THz pulse generation and detection, we use T-Ray 4000 TD-THz System from PICOMETRIX [5]. The interchangeable fiber-coupled sensor heads deliver a picosecond duration time-domain THz pulse. Fig. 6 depicts our ultra-broadband transceiver system and its generated THz pulse in time and frequency domains.

Fig. 7 shows our measurement setup. We first generate a THz pulse and focus it to the LWA via a lens with a focal distance of 6 cm.

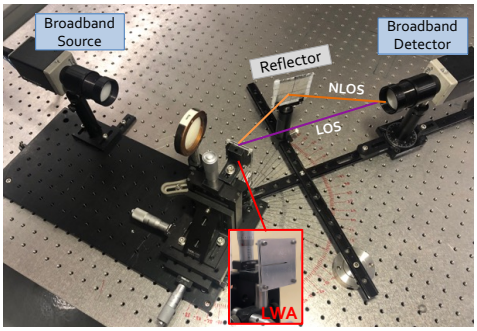

Figure 7: Our experimental setup.

The signal leaking out of the waveguide generates a THz Rainbow. We exploit aluminum sheet as reflector to configure NLOS paths. To achieve different NLOS angles, we mount and move the reflector on a rail as shown in Fig. 7. Similarly, to vary the LOS angle, we mount the broadband detector on a rotating arm that rotates around the center of LWA. The broadband detector provides raw measurements of the composite received signals in time and frequency domains. In our experiments, we limit the setup to one-path (LOS or NLOS) and two-path settings and leave exploration of more complex THz channels for future work.

Due to hardware limitations, i.e., low-power THz source, we are bound to conduct experiments in small scales (up to a meter). Scaling up the transmitter-receiver distance is feasible by increasing the power emitted by the transmitter. In particular, our THz source emits an average power of roughly -10 dBm, which is the time-averaged power, integrating over the entire (1 THz) spectral band. Hence, the power in a 1 kHz bandwidth is -100 dBm. Meanwhile, prior work reported a CMOS-based widely tunable source which achieves about -10 dBm in a 1 kHz bandwidth, over the entire range 100-300 GHz offering a factor of 10^9 increase in output power compared to our THz source [4]. Further, links at WLAN-scale distances (100+ meters) have already been demonstrated at many frequencies between 100 GHz and 557 GHz [37] and in several bands at higher frequencies up to 850 GHz [38]. Note that increasing the transmit power does not affect the spatial-spectral signature of THz Rainbow nor the design of OPERA.

5 EVALUATION

In this section, we discuss our over-the-air experiments and evaluate the key components of OPERA.

5.1 Experimental Characterization of the THz Rainbow

We first experimentally characterize a THz Rainbow and validate the phenomenological model proposed in Sec. 3.

Setup. We deploy T-Ray 4000 THz system for THz pulse generation and broadband detection and integrate it with our LWA device. Fig. 8 depicts our experimental setup in which blue circles represent broadband detector locations. We conduct extensive experiments in multiple configurations covering different LWA-detector distances and relative angles. In each setting, we move the detector on a quadrant from 10° to 80° with the setup

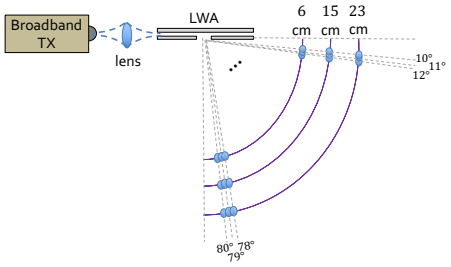

Figure 8: The schematic setup for THz Rainbow characterization.

of 1°. We explore this angular range since we observe that below 10° and above 80°, the leaked waves are fundamentally very weak (close to noise floor), due to a decrease in the efficiency of coupling from the guided wave to free space near the extrema of the angular range.

Methodology. In each setting, we identify the time window that the signal falls into through energy detection at our broadband detector. Then we lock the receiver to that time window and collect raw time-domain and frequency-domain data and apply signal processing techniques (such as smoothing, filtering, FFT, etc.).

5.1.1 Measuring The Angle-Frequency Relation. We first experimentally explore the angle-frequency coupling and compare it against the first principles model in Eq. (1). Fig. 9 plots the peak frequency of power spectrum vs. receiver's angle. The results show good agreement between the theory and experiment, at least for the angles above 20°. However, below 20°, the measurement results deviate from theoretical behavior. The reason is that, for those lower angles, the corresponding peak frequencies are above 400 GHz and higher frequency components are fundamentally weaker, even in the spectrum of THz illumination source (see the spectrum of THz pulse in Fig. 6). Hence, when exposed to path loss and coupling loss, the signal level degrades to the noise level increasing the measurement error. Also the model in Eq. (1) does not account for the realistic plate geometry. Namely, the non-idealities in the waveguide geometry such as the finite non-zero plate thickness contribute to a more complex spectrum, and these effects are likely to become more pronounced at small angles, where the effective propagation length inside the leaky-wave slot is larger.

Our results above show that the *peak frequency* (or the frequency that is maximally coupled) at a given angle matches the first principles model in Eq. (1). However, this model does not provide any information on other frequency components of the power spectrum. The overall spectral properties of waves composing a THz Rainbow is unexplored and no analytic solution exists even under idealistic geometry (i.e., zero plate thickness). In order to develop a phenomenological model, we directly measure the angular-dependent spectrum of a THz Rainbow, deploying the setup in Fig. 8.

Fig. 10 presents the heatmap of signal amplitude over different frequencies as a function of the LWA-receiver angle. For each frequency f, we normalize the corresponding amplitude over the entire angular range to the maximum value (i.e., normalizing every row of the heatmap matrix to the maximum value in that row). This

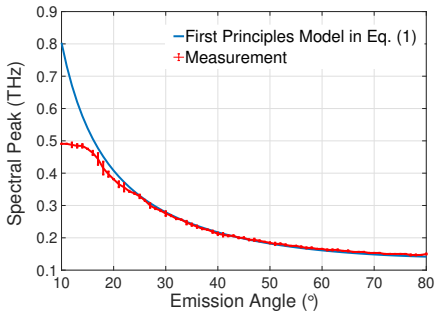

Figure 9: The LWA angle-frequency coupling, theory vs. experiment.

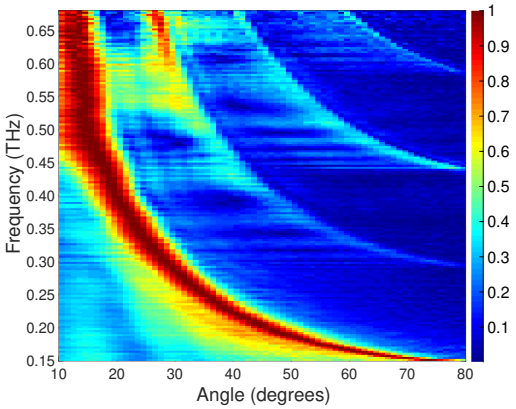

Figure 10: Spectrum-Angle heatmap of THz Rainbow.

heatmap includes the frequency range of 0.15 to 0.68 THz with the resolution of 3.1 GHz.

We observe that the high power region (with value one) follows Eq. (1). Interestingly, the heatmap shows high power associated with frequencies that are far from the frequency characterized by first principles model. In particular, at lower angles, the spectrum contains a wide range of high-power frequencies whereas at larger angles mostly frequencies close to 0.15 THz hold relatively high power (i.e., the yellow bright region is much wider for lower angles). Further, Fig. 10 reveals similar second-order and third-order higher frequency echos that are caused by higher order transverse electric (TE) modes in the waveguide.

Finding: We experimentally demonstrated THz Rainbow and showed that the peak frequency is inversely related to the angle of emission via a non-linear function. However, the overall spectral profile is irregular such that lower frequency components tend to spread over a wider range of angles.

5.1.2 Validation of our Phenomenological Model. In sec. 3, we modeled the THz Rainbow behavior as frequency-dependent spatial mask such that for a given frequency, the angular response is analogous to a spatial filter with a fall-off rate that itself depends on the frequency. To validate this model, we deploy the same setup as in Fig. 8 but this time we explore the change in the signal amplitude carried by frequency f as we deviate from the optimum angle. Even though our data set covers a wide range of frequencies, for

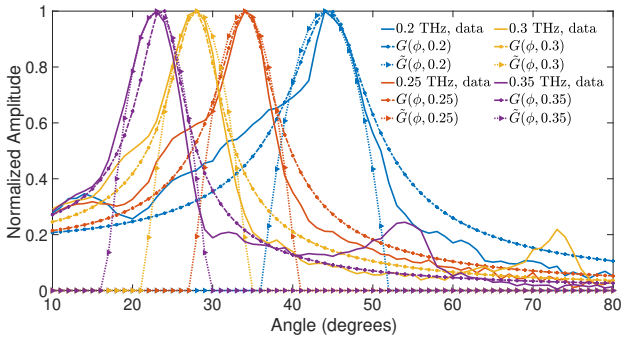

Figure 11: Validating the phenomenological model of spectral-spatial behavior in THz Rainbow.

the sake of space, we include results for few frequencies, namely, $f = 200, 250, 300$, and 350 GHz.

Fig. 11 depicts normalized measured amplitude together with the physical model $G(\phi, f)$ in Eq. (2) and our phenomenological model $\tilde{G}(\phi, f)$ in Eq. (3). The normalization is computed such that the best angle (for each frequency) has a peak value of one. We observe good agreement between the experimental data and the developed phenomenological model, at least for an angular range of interest (angles whose corresponding measured power is within the 3 dB of maximum power). For larger angular offsets, irregularities can be seen in the measured power that is not captured by our phenomenological model. The rationale is that the signal strength is substantially weaker with larger angular offset; thus, even if a more complex model is developed, it would not significantly improve the performance of OPERA.

Further, Fig. 11 confirms our approximation in Eq. (3) that the fall off rate (due to deviating from center angle on either side) is symmetric for the angular range of interest. Nonetheless, out of this range, we observe asymmetric behavior in a way that the fall off rate of the right tail is faster than the left tail. Finally, our experiments confirm that the fall-off rates are frequency-dependent such that the smaller the frequency, we observe less power drop given a fixed angular offset. We account for this dependency by including the frequency-dependent scalar $\gamma(f)$ in our expression in $\tilde{G}(\phi, f)$. Given a LWA device, $\gamma(f)$ is fixed and can be measured in advance.

Finding: We proposed and validated a model that characterizes the angular-dependent power spectral density of THz Rainbow. While the model does not capture the low-power irregularities at angles far from the optimum center angle, it accurately describes the power drop for a certain angular range of interest. OPERA takes advantage of such spatial-spectral signatures for path discovery.

5.2 OPERA Single-Path Discovery

We first evaluate the performance of OPERA in single-path settings (e.g., LOS or one reflected path only). For comparison purposes, we introduce a baseline scheme.

5.2.1 Baseline: Peak-Frequency Inversion. We introduce a baseline path discovery approach which we call Peak-Frequency Inversion. This scheme takes the spectral peak as signatures to find angle paths. The rationale is that the spectral peak has a one-to-one relation

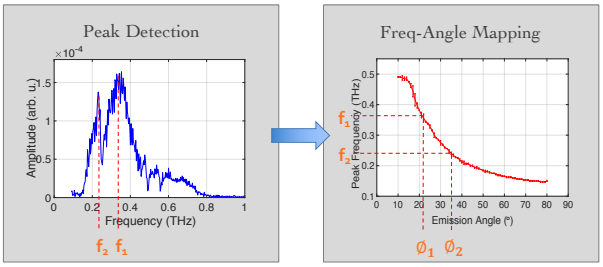

Figure 12: The baseline scheme that directly maps peaks in power spectrum to corresponding angles.

with the receiver's angle relative to the LWA. Besides, we expect paths to contribute to the overall spectrum based on their AoD, disregard of whether it is a LOS or a reflected path. In other words, we hypothesize that reflecting off a surface does not impact the spectral signature (in particular, the peak frequency) of the incident signal.

Fig. 12 describes the Peak-Frequency Inversion scheme consisting of a peak detection component and a frequency to angle mapping module. This scheme picks p frequencies, each corresponding to a path, from the received power spectrum and maps them to the corresponding angles. Our result in Sec. 5.1 revealed that the first principle model in Eq. (1) deviates from measurements for emission angles below 20 degrees. Hence, to eliminate this source of error, we exploit the measured angle-frequency curve in Peak-Frequency Inversion, as shown in Fig. 12.

The baseline scheme does not require any prior information other than the measured angle-frequency curve. Of course, one could even relax this constraint by substituting this measured curve with the Eq. (1), with the risk of higher estimation error for some path angles. Instead, OPERA assumes the spectral characteristics at different angles are known and exploits such signatures to find the path angles that best fits the entire power spectrum through a maximum likelihood optimization.

5.2.2 LOS vs. NLOS Detection. In this experiment, we compare the effectiveness of OPERA and Peak-Frequency Inversion in detection of a LOS path vs. a single reflected path. We consider various LOS settings with angles in the range of $15^\circ - 75^\circ$ and configure the setup carefully to ensure that no reflection exists. Each time, we excite the transmit LWA with a THz pulse and collect the signal received at the broadband detector. We repeat a similar experiment but this time we block the LOS path and carefully set up a metal reflector to add a reflected path. To compute the estimation error, we compare the predicted path direction with the geometric angle between the LWA and the center of the reflector.

Fig. 13 depicts the histograms of estimation error over different ground truth angular intervals for both LOS-only and NLOS-only experiments. In the LOS settings, i.e., Fig. 13a, we observe that the estimation error of Peak-Frequency Inversion is non-uniform across different angles and increases significantly for LOS angles above 55°. The reason is rooted in the non-linearity of frequency-angle relation in the LWAs. As shown in Fig. 9, the peak frequency is roughly a flat (or slowing varying) function of the emission angle for angles above 55 degrees; thus, a small measurement error in

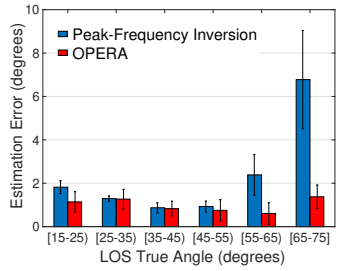

(a) Single LOS path

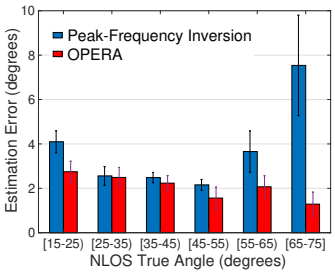

(b) Single NLOS path

Figure 13: The histogram of estimation error in single-path settings.

the spectral domain may cause significant error in angle estimates. Moreover, the spectral resolution of any broadband receiver is finite and bound to its clock sampling rate. The frequency resolution in our setup is 3.1 GHz; thus, peak frequency may be mistakenly shifted by up to 3.1 GHz and yield to an estimation error of several degrees in this slow-varying regime. In contrast, OPERA takes into account the spectral-angular profile of THz Rainbow and the relative power across different frequencies for path detection. Thus, it is able to distinguish between path angles with similar corresponding spectral peaks and consistently achieves less than 2° error on average across the angular space.

Fig. 13b reveals two key differences in NLOS detection: First, for both OPERA and baseline, the average estimation error is slightly higher in all angular intervals. Second, the Peak-Frequency Inversion approach obtains larger error at the two ends of the angular range, i.e., [15-25] and [65-75]. The reason is two-fold: given the same AoD, a reflected path endures higher loss due to the reflection loss and the increased path length. Hence, the NLOS path is weaker and prone to higher estimation error. Moreover, reflection imposes non-equal attenuation over different frequencies leading to spectral peak shift or generally adds noise to the spectral signature of the path. Higher frequency components are more exposed to these errors comparing to the lower frequencies because they endure higher reflection loss and path loss. Hence, from Fig. 13b, we observe that the baseline scheme obtains high errors for lower angles in the range of $15-25$ that contain higher frequency components. OPERA is not immune to the non-perfect reflection loss either; however, by considering the relative power over the entire power spectrum, it can better diminish the impact of such errors.

Finding: Even though the baseline scheme takes advantage of the one-to-one relation between spectral peak and emission angle, we find that it encounters critical limitations in practice. First, for a range of angles, the peak frequency is a slow-varying function of the emission angle makes it susceptible to measurement error and the limited frequency resolution at the receiver. Second, reflection non-uniformly impacts power over different frequencies which can lead to a spectral peak shift and subsequent estimation inaccuracy.

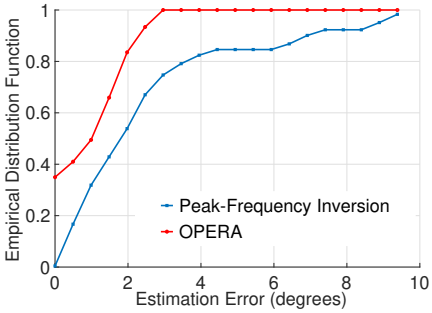

Figure 14: The estimation accuracy of OPERA in single-path settings.

5.2.3 Single-Path Estimation Accuracy. Next, we explore the overall performance of OPERA vs. Peak-Frequency Inversion in single-path extraction (LOS-only and NLOS-only combined). We choose 225 different configurations in which the ground truth AoD varies between 10 to 80 degrees. Fig. 14 presents the empirical distribution function of the estimation error, which is the number of observations less than or equal to a specific error divided by the total 225 independent measurement readings.

The result reveals that OPERA successfully estimates the AoD within 2.2 degrees of the ground truth in 90% of cases. In addition, a simple frequency to angle mapping as in baseline achieves less than 3.8 degrees error in 80% of cases. Nonetheless, its curve slowly approaches one; in particular, in 18% of single-path settings the estimation error was more than 6 degrees and in 10% of instances the error was higher than 8 degrees. From the above analysis, we know that these high-error cases correspond to larger LOS/NLOS angles.

Finding: In single-path channels, Peak-Frequency Inversion achieves on average a comparable performance with OPERA. Yet, its accuracy is not robust across the entire angular domain.

5.3 OPERA Multipath Extraction

In multi-path channels, the receiver captures a superposition of signals traveling along different paths. In OPERA, by design, the spectral properties of such signals are unique when emitted from the LWA. However, the key question is whether or not such spatial-spectral signatures are reliably extractable from the superposed signal in multipath settings.

Setup. We consider two-path configurations, with one LOS and one reflected path. The schematic of our multipath experimental setup is shown in Fig. 15. We set an aluminum sheet as reflector and slide it on a rail to vary the NLOS path angle. This rail is attached to another fixed rail at cross point C such that the distance from LWA to C is equal to RX to point C distance. Furthermore, the reflector is oriented in parallel to the rail that connects LWA to the RX. These considerations ensure that the portion of the emitted THz Rainbow

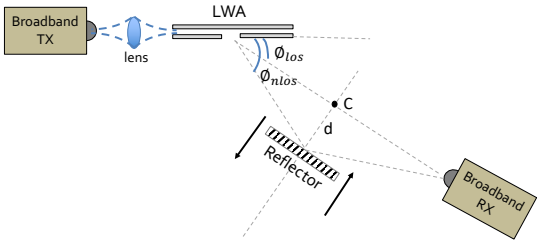

Figure 15: The schematic of our multipath experimental setup.

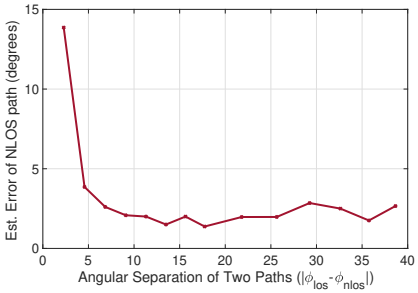

Figure 16: The estimation error of the reflected path as a function of inter-path angular separation.

that reflects off the reflector can be collected by the broadband RX. Moving the reflector from point C to the left increases the NLOS angle ($\phi_{nlos} > \phi_{los}$) and vice versa.

5.3.1 Minimum Inter-Path Angular Separation. OPERA identifies different paths via their angular-dependent frequency signature. Thus, when two paths have close AoD, their spectral profile might be indistinguishable. Hence, one key evaluation factor is the minimum required angular separation between paths so that we can successfully extract their signatures from the superposed received signal.

To answer this question, we consider a fixed LOS configuration with path angle ϕ_{los} and move the reflector along the rail in the steps of 5 cm to vary the angular separation between the LOS and reflected path (i.e., $|\phi_{los} - \phi_{nlos}|$). We repeat this experiment for a discrete choice of LOS angles (i.e., ϕ_{los}=15 to 75 in steps of 5 degrees). At each multipath setting, we collect raw data from the broadband receiver and implement OPERA path discovery.

We find that LOS detection is robust to inter-path angular separation. The reason is that the LOS path is stronger and its spectral signature dominates the characteristics of the received signal. However, Fig. 16 reveals this does not hold true for the reflected path. This figure shows the estimation error associated with detection of the NLOS path vs. the inter-path angular separation. We observe that when paths are not sufficiently separated (e.g., $|\phi_{los} - \phi_{nlos}| < 3°$), the estimation error is significantly high. Since paths have similar spectral signatures in such cases, removing the contribution of first path from the superposed signal disrupts the detection of the second path.

Finding: When multiple paths are sufficiently angularly separated, i.e., $|\phi_{los} - \phi_{nlos}| > 3°$, OPERA can successfully extract their spatial-spectral signatures.

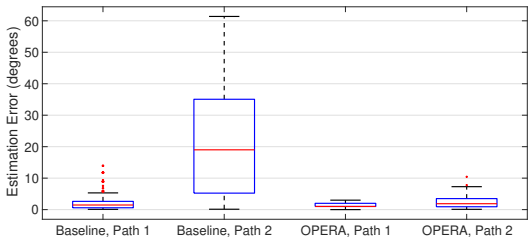

Figure 17: The box plot of estimation error for more than 300 independent multipath configurations.

5.3.2 Overall Multi-Path Estimation Accuracy. Finally, we analyze the overall performance of OPERA compared to the Peak-Frequency Inversion approach in multipath discovery. Hence, we place the receiver in different LOS angles relative to the transmit LWA (from 15 to 75 in the steps of 5 degrees) and configure the reflector in multiple locations along the rail (in the steps of 5 cm) to create a range of NLOS angles. Fig. 17 shows the box plot of the estimation error for more than 300 independent multipath measurements.

The Peak-Frequency Inversion scheme offers a relatively comparable performance on average in the discovery of the LOS path; nonetheless, its accuracy is non-uniform across the entire angular domain leading to higher variance. More importantly, Peak-Frequency Inversion demonstrates unreliable performance in the extraction of the second path. The reason is rooted in the irregularities in the spatial-spectral signatures of THz Rainbow. In other words, if such signatures were indeed a sharp delta function (i.e., each frequency was emitted from one and only one direction), then Peak-Frequency Inversion performance would have been enhanced as the spectrum of different paths would have been completely isolated and non-interfering. Instead, each path contributes to the overall spectrum with its wide and irregular spectral signature. Further, such contributions are not equally strong. In particular, the spectral peak of a secondary path might get dissolved in the irregularities of a stronger LOS spectral signature. In contrast, OPERA exploits the fact that THz Rainbow spectral profile is fixed and can be known a priori; therefore, the receiver correlates its signal with the known but irregular transmission signatures; thus, it is able to detects the second path direction with only 1.9° error on average.

Finding: Irregularities in the THz Rainbow profile together with the non-equal path strengths cause inaccurate path estimation by Peak-Frequency Inversion in multi-path settings. Instead, OPERA exploits the known but irregular spectral signatures to successfully extract multiple paths.

5.4 OPERA for Beam Adaptation

Here, we evaluate the effectiveness of OPERA for beam adaptation. In particular, we explore two main factors: *(i)* The SNR penalty associated with non-ideal path estimates. This enables us to understand the performance penalty (ultimately in data rate) due to imperfect beam alignment. *(ii)* The rate at which path updates are provided, as stale path data can also degrade performance for mobile clients.

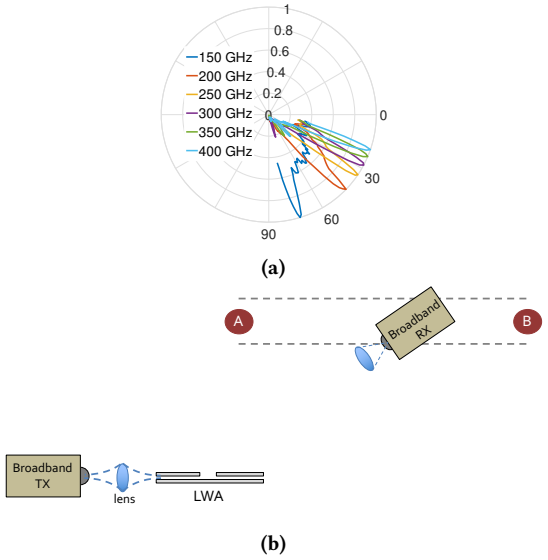

(a)

(b)

Figure 18: (a) Example directional radiation patterns generated by LWA; (b) Our mobility setup.

Figure 19: The SNR performance of beam adaptation when path directions are provided by OPERA.

5.4.1 SNR Performance. As discussed above, OPERA provide path directions within 2° of the ground truth. This non-zero error results in sub-optimal beam steering and an SNR penalty, consequently. We compare the SNR of OPERA beam adaptation with the maximum achievable SNR via an Oracle approach that has perfect knowledge of paths. Note that here, we assume the path tracking rate (the rate at which path information is updated) is exactly the same for Oracle and OPERA; hence, any difference in SNR is solely due to path estimation errors. Moreover, we expect the SNR difference to depend on the radiation patterns of directional beams in use, e.g., narrow beams are more sensitive to path estimation errors. Here, to have a fair comparison, we obtain a set of fixed beam patterns for both Oracle and OPERA schemes. In particular, we generate directional beams with a LWA by tuning the carrier frequency of the input signal. Example radiation patterns are shown in Fig. 18a.

Setup. We deploy the experimental setup in Fig. 18b, such that the transmitter is fixed and is equipped with a LWA. The broadband receiver is moving on a line from A to B. To emulate continuous motion, we collect raw data at the RX with high granularity of every 0.5 cm movement. Further, we repeat the same experiment in multiple parallel motion lanes with different distance to the TX. To isolate sender-side beam steering, we manually align the broadband RX as it moves along the translational line.

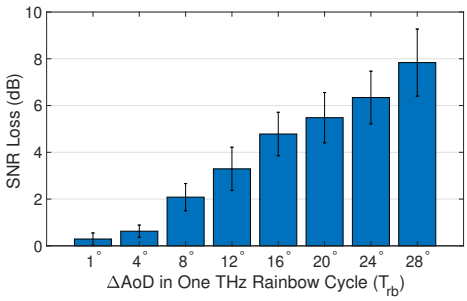

Figure 20: The impact of OPERA's path tracking rate on the accuracy of beam adaptation.

Fig. 19 plots the empirical distribution function of SNR loss in OPERA compared to the maximum achievable SNR via the Oracle Scheme. We observe the SNR loss of less than 2 dB in 90% of measurement instances. The non-zero error in AoD estimates yields to generation of a radiation pattern whose main-lobe is slightly misaligned from the ground truth angle and imposes an average SNR penalty of 0.3 dB

Finding: The non-zero error in path angle estimates provided by OPERA causes slightly misaligned beam steering, imposing an SNR penalty of 0.3 dB on average, comparing to the maximum achievable SNR via an Oracle scheme.

5.4.2 Path Tracking Rate. A key factor affecting beam adaptation performance is the rate at which path angle estimates are available. In Sec. 3, we demonstrated that OPERA includes the periodic transmissions of THz Rainbow in time intervals of T_{rb}. Such broadband transmissions occupy the entire spectral band yet only for a nano-second scale period of time. Data transmissions in all bands need be stopped or will otherwise interfere with path discovery and vice versa. Moreover, the translational speed of the client also affects steering accuracy; the faster the speed, the harder the tracking since the client's angular position may change more for the same estimation interval T_{rb}. Instead of evaluating these two factors separately, we consider the amount of change in client position relative to the transmitter during one cycle of OPERA, i.e., T_{rb}.

Fig. 20 presents SNR loss for different client movements in T_{rb}. The AoD of the LOS path varies as the client moves along the translational line. We use ΔAoD (between two consecutive THz Rainbows) as a metric for how fast the client moves since changes in the AoD indicate whether the transmit beam needs to be adapted or not. A larger number on the x-axis means that either T_{rb} is larger (for the same client speed) or the client is moving faster (for the same T_{rb}).

We observe that when path tracking is repeated most frequently (every 1° of client angular movement), the SNR loss (compared to the maximum achieved SNR via the Oracle scheme) is the lowest. Since the path angle estimates are being updated faster, we can adapt beams before client moves out of the AP's steering direction and experiences a significant SNR loss. We observe that in such a case, the average SNR loss is only 0.29 dB. Furthermore, as the estimation interval increases, the average SNR loss also becomes large, since there is a great change in AoD between two path discovery measurements.

As discussed in Section 3.4.3, THz Rainbow transmission incurs nanosecond-scale overhead whereas mobility is in millisecond time scales. For instance, consider a mobile client who is moving with speed of 10 m/s on a translation line with initial distance of 10 m from the transmit LWA. Then, the most frequent path tracking (i.e., every 1° of client movement) requires T_{rb} to be 17 msec meaning path directions need to be updated in millisecond-scale.

Finding: When the THz Rainbow is generated more frequently, the average SNR loss at a mobile client is smaller as beams can be better adapted based on the latest path directions. Yet, even under intensive path tracking (e.g., for every 1° change of client movement), the time overhead of updating paths is orders of magnitude smaller than the mobility scale.

6 RELATED WORK

Leaky Wave Antennas. LWAs have a long history, having been used in the RF region since at least the 1940's [2]. Most early examples were rectangular waveguides; however, in the THz range, the parallel-plate waveguide has been shown to be a very useful low-loss and low-dispersion platform for many purposes [15, 19]. While LWAs facilitate beam steering toward a specific direction, discovering the right beam direction at the TX and RX remains a challenge in the literature. This work is the first-ever use of LWA devices as control plane to adapt THz WLANs and the first to use the LWA to transmit in all directions simultaneously.

Path Discovery. Prior work focuses on AOA estimation by exploiting large antenna arrays and taking advantage of advanced signal processing techniques [35, 36]. In particular, such approaches employ the phase difference at multiple antennas to infer the direction of wave incident. However, this method is not applicable in THz bands as even the state of the art THz node architecture cannot provide the amplitude and phase information corresponding to each antenna element in an antenna array.

More recent work proposed an alternative approach to direction finding using a time-modulated array. In this technique, by periodic on-off switching of the array elements, harmonic components are generated and analyzed to estimate the arrival direction. Compared with the aforementioned array-based AOA estimation techniques, the time-modulated array offers high precision, while its hardware complexity and calculation complexity are relatively low [27, 33]. However, the application of time-modulated arrays in high-frequency regimes is limited by the speed of RF switches. Further, this approach requires periodic transmission of the signal under different switching states and thus it is clearly not a single-shot nor a single-antenna approach.

Another body of work uses visible light sensing to estimate the AoA of the LOS path between the light source and a photodiode array at the client [10, 16]; however, such approaches are limited to the LOS path only. Authors in [26] study non-coherent path tracking in mmWave but their approach requires multiple beacon transmissions. Path angle estimation for THz communication has been studied recently in [25], in which the authors utilize a low frequency RF frontend to roughly estimate the AOA in a first step and refine it in THz regime in a second step. In contrast, our work proposes a single-shot and single antenna path discovery scheme that can identify all dominant paths between the AP and all clients.

Finally, a recent work in 60 GHz networks exploits the irregularity and side-lobes in 60 GHz beam patterns together with power delay profile measurements for path identification [8]. In contrast to practical antenna arrays in 60 GHz with wide and irregular beam patterns, THz beams are regularly shaped and quite narrow [6].

Directional Neighbor Discovery. Several papers addressed the problem of neighbor discovery for wireless networks that use directional antennas [21, 22, 40]. Their main objective is to discover the neighbors, i.e., nodes that are within communication range, around any particular node and store the neighborhood information. In particular, the challenge is to quickly steer the listening beam direction so that it can decode any of the multiple beacons transmitted directionally in a multi-shot discovery procedure. Instead, OPERA attempts to characterize all dominant paths between two nodes via one-shot transmission. Nonetheless, OPERA can be employed for directional neighbor discovery as well. To this end, the node aiming to identify its neighbors has to transmit a THz Rainbow. When OPERA identifies a path at a particular receiving node, one can conclude that those nodes are neighbors.

mmWave Beam Adaptation. There is extensive work to reduce overhead of beam acquisition and adaptation in mmWave networks. Beam acquisition solutions include IEEE 802.11ad/ay's sector sweeping [7, 23], hierarchical codebook designs [1, 12], compressive sensing techniques to exploit channel sparsity [17, 30] and model-driven beam steering via channel profiling [34, 41]. For beam adaptation under mobility prior work suggests a variety of in-band and out-of-band solutions including the use of legacy bands [24, 32] or visible light [10], and efficient beam searching [11, 39]. These efforts reduce training overhead and maintain alignment for mmWave links. However, given that THz links lack the "pseudo-omni" reception capability available at mmWave and are inherently more directional, these solutions are not applicable in THz bands. In contrast, this work provides path directions and enables efficient beam steering and beam adaptation in THz Networks.

7 CONCLUSION

In this paper, we present OPERA, a novel single-shot single-antenna system that enables the discovery of dominant LOS and NLOS paths in THz channels. OPERA embeds path direction information into the inherent characteristics of the signal traveling along that path. In particular, we create a THz Rainbow by exciting a single leaky wave antenna with a THz pulse and simultaneously transmit signals whose spectral signatures are a function of emission angle. We model such angular-dependent signatures in order to enable the receiver to extract path directions from the received power spectrum. Our experiments show that OPERA achieves direction estimates within 2° of ground truth on average while incurring only tens of nano second overhead.

8 ACKNOWLEDGMENTS

We appreciate the valuable comments and feedback from the anonymous reviewers. This research was supported by Intel, and by NSF grants CNS-1642929, CNS-1514285, CNS-1629929, and CNS-1553447.

REFERENCES

[1] Ahmed Alkhateeb, Omar El Ayach, Geert Leus, and Robert W Heath. 2014. Channel Estimation and Hybrid Precoding for Millimeter Wave Cellular Systems. *IEEE Journal of Selected Topics in Signal Processing* 8, 5 (2014), 831–846.

[2] Constantine A Balanis and Craig R Birtcher. 2008. Antenna Measurements. *Modern Antenna Handbook* (2008), 977–1033.

[3] Matthew C Beard, Gordon M Turner, and Charles A Schmuttenmaer. 2002. Terahertz Spectroscopy.

[4] Taiyun Chi, Min-Yu Huang, Sensen Li, and Hua Wang. 2017. 17.7 A Packaged 90-to-300GHz Transmitter and 115-to-325GHz Coherent Receiver in CMOS for Full-Band Continuous-wave mm-Wave Hyperspectral Imaging. In *Proc. of IEEE ISSCC*.

[5] Irl Duling and David Zimdars. 2009. Terahertz Imaging: Revealing Hidden Defects. *Nature Photonics* 3, 11 (2009), 630.

[6] John Federici and Lothar Moeller. 2010. Review of Terahertz and Subterahertz Wireless Communications. *Journal of Applied Physics* 107, 11 (2010), 6.

[7] Yasaman Ghasempour, Claudio da Silva, Carlos Cordeiro, and Edward W. Knightly. 2017. IEEE 802.11ay: Next-generation 60 GHz Communication for 100 Gbps Wi-Fi. *IEEE Communications Magazine* 55, 12 (2017), 186–192.

[8] Yasaman Ghasempour, Muhammad K. Haider, Carlos Cordeiro, Dimitrios Koutsonikolas, and Edward Knightly. 2018. Multi-Stream Beam-Training for mmWave MIMO Networks. In *Proc. of ACM MobiCom*.

[9] Frank B. Gross. 2011. *Frontiers in Antennas: Next Generation Design & Engineering*. McGraw-Hill Education.

[10] Muhammad Kumail Haider, Yasaman Ghasempour, Dimitrios Koutsonikolas, and Edward W. Knightly. 2018. LiSteer: MmWave Beam Acquisition and Steering by Tracking Indicator LEDs on Wireless APs. In *Proc. of ACM MobiCom*.

[11] Haitham Hassanieh, Omid Abari, Michael Rodriguez, Mohammed Abdelghany, Dina Katabi, and Piotr Indyk. 2018. Fast Millimeter Wave Beam Alignment. In *Proc. of ACM SIGCOMM*.

[12] Sooyoung Hur, Taejoon Kim, David J Love, James V Krogmeier, Timothy A Thomas, and Amitava Ghosh. 2013. Millimeter Wave Beamforming for Wireless Backhaul and Access in Small Cell Networks. *IEEE Transactions on Communications* 61, 10 (2013), 4391–4403.

[13] David R. Jackson and Arthur A. Oliner. 2008. Leaky-Wave Antennas. *Modern Antenna Handbook* (2008), 325–367.

[14] Nicholas Karl, Martin S Heimbeck, Henry O Everitt, Hou-Tong Chen, Antoinette J Taylor, Igal Brener, Alexander Benz, John L Reno, Rajind Mendis, and Daniel M Mittleman. 2017. Characterization of an Active Metasurface using Terahertz Ellipsometry. *Applied Physics Letters* 111, 19 (2017), 191101.

[15] Nicholas J Karl, Robert W McKinney, Yasuaki Monnai, Rajind Mendis, and Daniel M Mittleman. 2015. Frequency-division Multiplexing in the Terahertz Range using a Leaky-wave Antenna. *Nature Photonics* 9, 11 (2015), 717.

[16] Ye-Sheng Kuo, Pat Pannuto, Ko-Jen Hsiao, and Prabal Dutta. 2014. Luxapose: Indoor Positioning with Mobile Phones and Visible Light. In *Proc. of ACM MobiCom*.

[17] Zhinus Marzi, Dinesh Ramasamy, and Upamanyu Madhow. 2016. Compressive Channel Estimation and Tracking for Large Arrays in mm-Wave Picocells. *IEEE Journal of Selected Topics in Signal Processing* 10, 3 (2016), 514–527.

[18] Marx Mbonye, Rajind Mendis, and Daniel M Mittleman. 2013. Measuring TE 1 Mode Losses in Terahertz Parallel-Plate Waveguides. *Journal of Infrared, Millimeter, and Terahertz Waves* 34, 7-8 (2013), 416–422.

[19] Rajind Mendis, Abhishek Nag, Frank Chen, and Daniel M Mittleman. 2010. A Tunable Universal Terahertz Filter using Artificial Dielectrics based on Parallel-Plate Waveguides. *Applied physics letters* 97, 13 (2010), 131106.

[20] Anamaria Moldovan, Michael A. Ruder, Ian F. Akyildiz, and Wolfgang H. Gerstacker. 2014. LOS and NLOS Channel Modeling for Terahertz Wireless Communication with Scattered Rays. In *IEEE Globecom Workshops*.

[21] Robert Murawski, Emad Felemban, Eylem Ekici, Sangjoon Park, S Yoo, Kangwoo Lee, Juderk Park, and Z Hameed Mir. 2012. Neighbor Discovery in Wireless Networks with Sectored Antennas. *Ad hoc networks* 10, 1 (2012), 1–18.

[22] Jianxia Ning, Tae-Suk Kim, Srikanth V. Krishnamurthy, and Carlos Cordeiro. 2009. Directional Neighbor Discovery in 60 GHz Indoor Wireless Networks. In *Proceedings of the 12th ACM International Conference on Modeling, Analysis and Simulation of Wireless and Mobile Systems (MSWiM '09)*.

[23] Thomas Nitsche, Carlos Cordeiro, Adriana B. Flores, Edward W. Knightly, Eldad Perahia, and Joerg Widmer. 2014. IEEE 802.11ad: Directional 60 GHz Communication for Multi-Gigabit-per-second Wi-Fi. *IEEE Communications Magazine* (2014).

[24] Thomas Nitsche, Adriana B. Flores, Edward W. Knightly, and Joerg Widmer. 2015. Steering with Eyes Closed: mm-Wave Beam Steering without In-Band Measurement. In *Proc. of IEEE INFOCOM*.

[25] Bile Peng, Ke Guan, Sebastian Rey, and Thomas Kurner. 2018. Two-Step Angle-of-Arrival Estimation for Terahertz Communications based on Correlation of Power-Angular Spectra in Frequency. In *In Proc. of EuCAP*.

[26] Maryam Eslami Rasekh, Zhinus Marzi, Yanzi Zhu, Upamanyu Madhow, and Haitao Zheng. 2017. Noncoherent mmWave Path Tracking. In *Proc. of HotMobile*.

[27] Paolo Rocca, Lorenzo Poli, and Andrea Massa. 2012. Instantaneous directivity optimisation in time-modulated array receivers. *IET Microwaves, Antennas & Propagation* 6, 14 (2012), 1590–1597.

[28] Swetank Kumar Saha, Yasaman Ghasempour, Muhammad Kumail Haider, Tariq Siddiqui, Paulo De Melo, Neerad Somanchi, Luke Zakrajsek, Arjun Singh, Owen Torres, Daniel Uvaydov, Josep Miquel Jornet, Edward Knightly, Dimitrios Koutsonikolas, Dimitris Pados, and Zhi Sun. 2017. X60: A Programmable Testbed for Wideband 60 GHz WLANs with Phased Arrays. In *Proc. of ACM WiNTECH*.

[29] Kaushik Sengupta and Ali Hajimiri. 2012. A 0.28 THz Power-Generation and Beam-Steering Array in CMOS based on Distributed Active Radiators. *IEEE Journal of Solid-State Circuits* 47, 12 (2012), 3013–3031.

[30] Daniel Steinmetzer, Daniel Wegemer, Matthias Schulz, Joerg Widmer, and Matthias Hollick. 2017. Compressive Millimeter-Wave Sector Selection in Off-the-Shelf IEEE 802.11 ad Devices. In *Proc. of ACM CoNEXT*.

[31] Daniel Steinmetzer, Daniel Wegemer, Matthias Schulz, Joerg Widmer, and Matthias Hollick. 2017. Compressive Millimeter-Wave Sector Selection in Off-the-Shelf IEEE 802.11ad Devices. In *Proc. of ACM CoNEXT*.

[32] Sanjib Sur, Ioannis Pefkianakis, Xinyu Zhang, and Kyu-Han Kim. 2017. WiFi-Assisted 60 GHz Wireless Networks. In *Proc. of ACM MobiCom*.

[33] Wen-Qin Wang, Hing Cheung So, and Alfonso Farina. 2017. An Overview on Time/Frequency Modulated Array Processing. *IEEE Journal of Selected Topics in Signal Processing* 11, 2 (2017), 228–246.

[34] Teng Wei, Anfu Zhou, and Xinyu Zhang. 2017. Facilitating Robust 60 GHz Network Deployment by Sensing Ambient Reflectors. In *Proc. of NSDI*.

[35] Carl Wong, Richard Klukas, and Geoffrey G. Messier. 2008. Using WLAN Infrastructure for Angle-of-Arrival Indoor User Location. In *Proc. of IEEE VTC*.

[36] Jie Xiong and Kyle Jamieson. 2013. ArrayTrack: A Fine-grained Indoor Location System. In *Proc. of NSDI*.

[37] Yihong Yang, Mahboubeh Mandehgar, and Daniel R. Grischkowsky. 2012. Understanding THz Pulse Propagation in the Atmosphere. *IEEE Transactions on Terahertz Science and Technology* 2, 4 (2012), 406–415.

[38] Yihong Yang, Mahboubeh Mandehgar, and Daniel R. Grischkowsky. 2015. THz-TDS Characterization of the Digital Communication Channels of the Atmosphere and the Enabled Applications. *Journal of Infrared, Millimeter, and Terahertz Waves* 36, 1 (2015), 97–129.

[39] Zhicheng Yang, Parth H. Pathak, Zeng. Yunze, and Prasant Mohapatra. 2015. Sensor-Assisted Codebook-Based Beamforming for Mobility Management in 60 GHz WLANs. In *Proc. of IEEE MASS*.

[40] Anfu Zhou, Teng Wei, Xinyu Zhang, and Huadong Ma. 2018. FastND: Accelerating Directional Neighbor Discovery for 60-GHz Millimeter-Wave Wireless Networks. *IEEE/ACM Transactions on Networking*. 26, 5 (2018), 2282–2295.

[41] Anfu Zhou, Xinyu Zhang, and Huadong Ma. 2017. Beam-forecast: Facilitating Mobile 60 GHz Networks via Model-driven Beam Steering. In *Proc. of IEEE INFOCOM*.